Available online at www.sciencedirect.com
SCIENCE DIRECT®
Applied Numerical Mathematics 50 (2004) 15–47
APPLIED NUMERICAL MATHEMATICS
www.elsevier.com/locate/apnum

Analytical study of the effect of wave number on the performance of local absorbing boundary conditions for acoustic scattering

Isaac Harari [a,*,1], Rabia Djellouli [b,2]

[a] *Department of Solid Mechanics, Materials, and Systems, Tel Aviv University, 69978 Ramat Aviv, Israel*
[b] *Department of Mathematics, California State University Northridge, Northridge, CA 91330-8313, USA*

Available online 17 January 2004

Abstract

The computation of exterior wave problems at low wave numbers can become prohibitively expensive when higher circumferential modes are significant. An analysis of the effect of wave number on scattering problems, with local absorbing boundary conditions specified on simple shapes as on-surface radiation conditions, provides guidelines for satisfactory performance. Excessive computational cost may be avoided for most practical applications.

Keywords: Wave number; Absorbing boundary conditions; Acoustic scattering

1. Introduction

Artificial boundaries are introduced in exterior problems in order to form bounded computational domains that are suitable for domain-based discretization. Correct far-field behavior is then enforced either by specifying proper boundary conditions on this boundary, or by assuming interpolation with suitable behavior in the complement of the computational domain [1]. The latter approach is associated with 'infinite elements' [2–6]. On the other hand, artificial boundary conditions (ABC) refer to a class of methods that is based on specifying proper boundary conditions on the artificial boundary. The terms

* Corresponding author.
E-mail addresses: harari@eng.tau.ac.il (I. Harari), rabia.djellouli@csun.edu (R. Djellouli).
URL: http://www.eng.tau.ac.il/~harari (I. Harari).

[1] This work was done in part while the author was visiting the University of Colorado at Boulder.

[2] This work was done while the author was at the University of Colorado at Boulder.

0168-9274/$30.00
doi:10.1016/j.apnum.2003.11.007

'radiation', 'nonreflecting', or 'absorbing' boundary conditions are used in the context of exterior wave problems.

Absorbing boundary conditions can be either exact or approximate. The former representations (which are usually global) are often termed exact even though they are typically expressed as infinite series, e.g., [7–10], which in practice are truncated to a finite number of terms. Nonetheless, the order is easily increased to almost any desirable level. On the other hand, straightforward implementation of approximate boundary conditions in standard (C^0) finite element methods is typically restricted to lower-order conditions, usually second order, due to continuity constraints. While there are advantages to the so-called exact interface representations, approximate boundary conditions are more commonly employed in practice due to a variety of reasons [11], primarily simplicity, locality, and applicability to general shapes of artificial boundaries. This paper presents an analysis of the effect of *low* wave number on scattering problems, with local absorbing boundary conditions specified on simple shapes as on-surface radiation conditions, providing guidelines for satisfactory performance on the simple cylindrical and spherical geometries considered.

The development of approximate, local boundary conditions is ongoing, e.g., [12–17]. In the following, we pay particular attention to the widely-used Bayliss–Gunzburger–Turkel (BGT) conditions [13], and the local Dirichlet-to-Neumann (DtN) boundary conditions [15,18], reviewed in Section 3. When employed on an artificial boundary in conjunction with finite elements, these boundary conditions are known to perform well for high wave numbers. This conclusion has been demonstrated, for example, for BGT, both analytically [13] and numerically [19–21].

In Section 4 we review analysis of absorbing boundary conditions, specified as on-surface radiation conditions (OSRC) for single mode *radiation* from simple shapes, showing that their performance indeed deteriorates at lower wave numbers, particularly for higher modes. The OSRC-based methods were originally developed for two-dimensional scattering problems [22]. The principle of these approaches is to solve a system of two boundary equations where the unknowns are the traces of the scattered field on the surface of the scatterer. The first equation characterizes the physical nature of the scatterer (the boundary condition) and the second one is the absorbing boundary condition (ABC) set on the surface of the scatterer. This approach leads to a sparse system of equations when both boundary equations are discretized by the finite element method. However, OSRC-based methods are efficient only for convex scatterers [23]. More analysis of OSRC implementations for scattering problems can be found in [24, 25]. Here, we adopt the OSRC approach to investigate analytically the performance of BGT and DtN boundary conditions for low wave numbers. which are a concern for finite element implementations. It is generally agreed (and confirmed by our results in Section 4) that for low wave numbers, accurate computation of radiation problems with low-order approximate absorbing boundary conditions can become prohibitively expensive when higher circumferential modes are significant. Extensive numerical comparisons of both boundary conditions at low wave numbers are reported in [26].

A similar analysis for *scattering* problems is performed in Section 5. Analysis of OSRC implementations for scattering problems is presented in [24,25]. The concern for implementation on an artificial boundary with finite elements is for low wave numbers. Here, the analysis shows that the range of satisfactory performance extends to relatively low wave numbers in this case, as was shown in passing in [27]. In qualitative terms this result, stating that for scattering high modes are less significant at low wave numbers, is expected. The analysis herein shows that the reduced significance of high modes at low wave numbers applies to problems with exact representations as well as with approximate boundary conditions. Furthermore, we are able to quantify this effect, providing guidelines for practical computa-

tion. The guidelines indicate that the range of low wave numbers at which satisfactory performance is still retained is as low as would be required in most practical acoustic scattering applications.

2. Exterior problems of time-harmonic acoustics

Let $\mathcal{R} \subset \mathbb{R}^d$ be a d-dimensional unbounded region. The boundary of $\mathcal{R}$, denoted by Γ, is *internal* and assumed piecewise smooth (Fig. 1). The outward unit vector normal to Γ is denoted by $\boldsymbol{n}$.

We consider a boundary-value problem related to acoustic radiation and scattering governed by the Helmholtz equation: find $u : \overline{\mathcal{R}} \to \mathbb{C}$, the spatial component of the acoustic pressure or velocity potential, such that

$$-\Delta u - k^2 u = f \quad \text{in } \mathcal{R}, \tag{1}$$

$$u = 0 \quad \text{on } \Gamma, \tag{2}$$

$$\lim_{r\to\infty} r^{\frac{d-1}{2}} \left(\frac{\partial u}{\partial r} - \mathrm{i}ku \right) = 0. \tag{3}$$

Here, Δ is the Laplace operator and $k \in \mathbb{C}$ is the wave number, $\operatorname{Im} k \geqslant 0$; $\mathrm{i} = \sqrt{-1}$ is the imaginary unit; $r = |\boldsymbol{x}|$ is the distance from the origin, and $f : \mathcal{R} \to \mathbb{C}$ is prescribed. Homogeneous Dirichlet boundary conditions on the internal boundary Γ are considered for simplicity. The results presented herein apply to all types of admissible internal boundary conditions.

Eq. (3) is the *Sommerfeld radiation condition* and allows only outgoing waves proportional to $\exp(\mathrm{i}kr)$ at infinity. The radiation condition requires that energy flux at infinity be positive, thereby guaranteeing that the solution to the boundary-value problem (1)–(3) is unique. Appropriate representation of this condition is crucial to the reliability of any numerical formulation of the problem (1)–(3).

In scattering problems the acoustic field is decomposed into a known incident field u^{i} and a scattered field u, i.e., $u^{\mathrm{i}} + u$. The scattered field u satisfies the boundary-value problem (1)–(3). The homogeneous Dirichlet problem is called acoustically soft, and the Neumann problem is called hard. For extensive results on properties of solutions to the boundary-value problem (1)–(3) with particular reference to scattering see, e.g., [28–32].

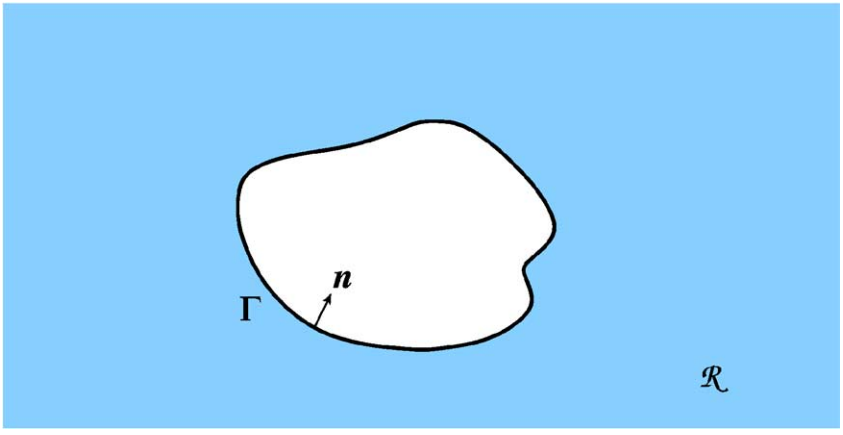

Fig. 1. An unbounded region with an internal boundary.

3. Measures of performance of absorbing boundary conditions

The unbounded domain $\mathcal{R}$ is truncated by an artificial boundary Γ_R (characterized by curvature $1/R$), yielding a bounded domain Ω that is suitable for direct discretization (Fig. 2). By analyzing the problem in the unbounded complement $\mathcal{R} \setminus \Omega$, boundary conditions involving a relation of the unknown solution and its derivatives are specified on Γ_R. This completes the definition of the boundary-value problem in Ω, which may now be solved by computation (e.g., with the finite element method). From this point onward k is taken to be a positive real number.

3.1. BGT boundary conditions

We consider BGT conditions [13], a sequence of boundary operators based on high kR asymptotics which provides increasingly accurate approximations to the problem in the unbounded domain. BGT conditions are widely used [19,33–35,21], and have recently been generalized to convex surfaces of arbitrary shapes [12].

Simply specifying the Sommerfeld condition on the artificial boundary

$$\text{BGT-0:} \qquad \frac{\partial u}{\partial r} = \mathrm{i}ku \quad \text{on } \Gamma_R, \tag{4}$$

can be considered a zero-order BGT condition (in the framework of the original sequence of operators [13]). This is known to be inaccurate for practical implementation.

BGT conditions of order higher than two are inappropriate for conventional finite element implementations since they require regularity higher than C^0. Consequently, we consider only the first (BGT-1) and second order (BGT-2) conditions in the following.

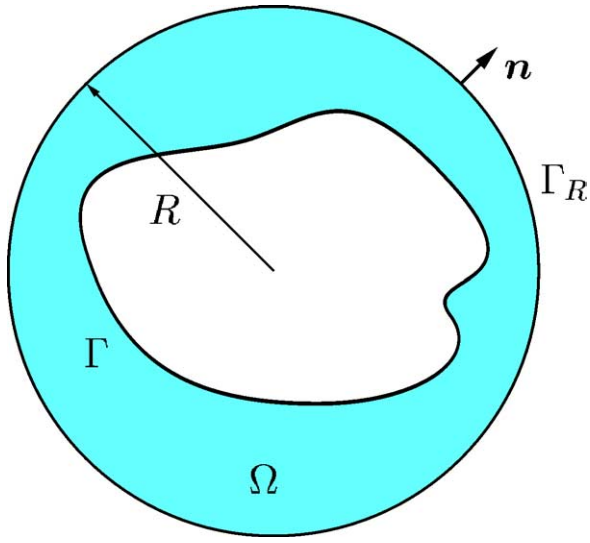

Fig. 2. The bounded computational domain.

3.1.1. Two dimensions

In polar coordinates, the two-dimensional BGT conditions [13] may be expressed as Robin boundary conditions on a circle of radius R (using the Helmholtz equation to eliminate the second radial derivative from BGT-2). Hence, on Γ_R we have

$$\text{BGT-1:} \qquad \frac{\partial u}{\partial r} = \left(\mathrm{i}k - \frac{1}{2R}\right)u, \tag{5}$$

$$\text{BGT-2:} \qquad \frac{\partial u}{\partial r} = \left(\mathrm{i}k - \frac{1}{2R} + \frac{1}{8R(1-\mathrm{i}kR)}\right)u + \frac{1}{2R(1-\mathrm{i}kR)}\frac{\partial^2 u}{\partial \theta^2}. \tag{6}$$

3.1.2. Three dimensions

We consider the spherical coordinate system (r,θ,ϕ), where $r \geqslant 0$ is the radial coordinate, $0 \leqslant \theta \leqslant 2\pi$ is the longitude or azimuth, and $0 \leqslant \phi \leqslant \pi$ is the polar angle or co-latitude. The three-dimensional BGT conditions [13] may be expressed as Robin boundary conditions on a sphere of radius R (using the Helmholtz equation to eliminate the second radial derivative from BGT-2). Hence, on Γ_R we have

$$\text{BGT-1:} \qquad \frac{\partial u}{\partial r} = \left(\mathrm{i}k - \frac{1}{R}\right)u, \tag{7}$$

$$\text{BGT-2:} \qquad \frac{\partial u}{\partial r} = \left(\mathrm{i}k - \frac{1}{R}\right)u + \frac{1}{2R(1-\mathrm{i}kR)}\Delta_s u. \tag{8}$$

Here, Δ_s is the Laplace–Beltrami operator, defined by

$$\Delta_s u = \frac{1}{\sin\phi}\frac{\partial}{\partial\phi}\left(\sin\phi\frac{\partial u}{\partial\phi}\right) + \frac{1}{\sin^2\phi}\frac{\partial^2 u}{\partial\theta^2}. \tag{9}$$

3.2. Local DtN boundary conditions

The truncated global DtN boundary condition ([11] and references therein) is localized, leading to a sequence of boundary conditions of increasing order that preserves exact representation of a finite number of lower modes. This procedure was proposed first for two dimensions [18], and later extended to three dimensions [36]. Details of derivation for different boundary-value problems, along with treatment of a variety of pertinent issues, are presented in [15].

As in the case of BGT conditions, local DtN conditions with more than two terms are inappropriate for conventional finite element implementations since they require regularity higher than C^0. Consequently, we consider only the one term (DtN-1) and two term (DtN-2) conditions in the following.

3.2.1. Two dimensions

In polar coordinates, the two-dimensional local DtN boundary conditions on Γ_R (a circle of radius R) are expressed as follows [18]

$$\text{DtN-1:} \qquad \frac{\partial u}{\partial r} = k\frac{H_0^{(1)'}(kR)}{H_0^{(1)}(kR)}u, \tag{10}$$

$$\text{DtN-2:} \qquad \frac{\partial u}{\partial r} = k\left(\frac{H_0^{(1)'}(kR)}{H_0^{(1)}(kR)}u + \left(\frac{H_0^{(1)'}(kR)}{H_0^{(1)}(kR)} - \frac{H_1^{(1)'}(kR)}{H_1^{(1)}(kR)}\right)\frac{\partial^2 u}{\partial\theta^2}\right). \tag{11}$$

Here, $H_n^{(1)}$ are n-order Hankel functions of the first kind. (See [37] for definitions and properties of special functions employed herein.) The prime on functions denotes differentiation with respect to the argument.

3.2.2. Three dimensions

In spherical coordinates, the three-dimensional local DtN boundary conditions on Γ_R (a sphere of radius R) are expressed as follows [36]

$$\text{DtN-1:} \qquad \frac{\partial u}{\partial r} = k\frac{h_0^{(1)'}(kR)}{h_0^{(1)}(kR)}u, \tag{12}$$

$$\text{DtN-2:} \qquad \frac{\partial u}{\partial r} = k\left(\frac{h_0^{(1)'}(kR)}{h_0^{(1)}(kR)}u + \frac{1}{2}\left(\frac{h_0^{(1)'}(kR)}{h_0^{(1)}(kR)} - \frac{h_1^{(1)'}(kR)}{h_1^{(1)}(kR)}\right)\Delta_s u\right). \tag{13}$$

The n-order spherical Hankel functions of the first kind satisfy

$$h_n^{(1)}(r) = \sqrt{\frac{\pi}{2r}}\, H_{n+1/2}^{(1)}(r). \tag{14}$$

The following result states the relation between BGT-n and DtN-n. (As noted above, the form of BGT-2 considered (8) is obtained by using the Helmholtz equation to eliminate the second radial derivative from the original definition [13].)

Proposition 3.2.1. *In three dimensions,* BGT-n *and* DtN-n *are identical for* $n = 1, 2$.

Proof. This result is a direct consequence of recursion properties of spherical Hankel functions [37, (10.1.22)]

$$h_n^{(1)'}(r) = \frac{n}{r}\, h_n^{(1)}(r) - h_{n+1}^{(1)}(r), \tag{15}$$

and the property

$$h_0^{(1)}(r) = -\mathrm{i}\exp(\mathrm{i}r)/r. \qquad \square \tag{16}$$

This connection was established in [38].

3.3. Measures of performance in OSRC context

The following analyses (Sections 4 and 5) evaluate the kR-dependence of the performance of local absorbing boundary conditions specified *on* simple shapes as on-surface radiation conditions (OSRC). The OSRC implementation is employed primarily as a tool to analyze the performance of the boundary conditions. In typical computation, the absorbing boundary conditions are specified on the artificial boundary Γ_R that bounds a computational domain Ω (Fig. 2) which is discretized by finite elements. In such implementations absorbing boundary conditions are known to perform well at high kR (specifically for BGT, see [13,19–21]). The failure of the lower-order absorbing boundary conditions to accurately capture highly directional solutions at high kR in some of the following analyses (which seems to counter intuition) has implications on the OSRC implementation only, as observed previously [23]. This difficulty

may be alleviated by employing higher-order radiation conditions [39], which are implemented in the OSRC context in straightforward manner.

When specified on an artificial boundary, increasing the size of the computational domain by increasing R (and thereby increasing kR), without modifying the physical boundary Γ, will improve the performance of the absorbing boundary condition, as expected [13,19–21]. The main interest in the following analyses is to evaluate the performance of the absorbing boundary conditions at *low* kR, to see if relatively small computational domains can be employed in order to avoid excessive computational cost.

In this paper we employ specific acoustic impedance, resistance, and inertia to evaluate the performance of BGT and local DtN conditions. The precision in which an absorbing boundary condition represents the unbounded medium may be assessed by comparing its specific acoustic impedance (the ratio of acoustic pressure to velocity) for given problems to exact values at various frequency regimes [40]. This approach is also used in the study of infinite elements [41–43].

Following [40], we introduce the ensuing non-dimensional quantities for the time-harmonic case considered herein:

Definition 3.3.1. The specific impedance is

$$z(\boldsymbol{x}) = \frac{\mathrm{i}ku}{\nabla u \cdot \boldsymbol{n}}. \tag{17}$$

Here, ∇ is the gradient operator. The specific impedance is a pointwise measure of the inverse of the normal derivative in the Dirichlet problems considered subsequently.

It is also convenient to consider separately:

Definition 3.3.2. The specific resistance

$$\eta = \operatorname{Re} z, \tag{18}$$

and the specific inertia

$$\mu = \frac{-1}{kR} \operatorname{Im} z. \tag{19}$$

As the names imply, these quantities measure the effect of the truncated medium in physical terms. Specific inertia is a non-dimensional measure of the ‘added mass’ of the surrounding medium. Specific resistance represents the radiative or damping effect. Use of these definitions is motivated in part by the limit behavior, particularly for axisymmetric spherical modes, see Eqs. (75)–(76). Inertial effects dominate the behavior at low wave numbers, while at high wave numbers resistance dominates. Exact values of these quantities are readily determined for simple configurations. Thus, these measures provide convenient indicators of the low- and high-frequency performance of a given approximate representation.

Following [44], we also introduce a measure which is a property of exact representations, and originates from electrical network synthesis:

Definition 3.3.3. A boundary condition is labeled passive when its specific resistance is positive, i.e., $\eta > 0$.

4. Performance of ABC for single mode radiation

Most of the experience on employing specific impedance to evaluate absorbing boundary conditions is based on problems of single mode radiation. The dependence of the specific impedance in such problems on the mode number n is denoted

$$z = z_n(kR). \tag{20}$$

Here, n is a nonnegative integer, unless specified otherwise. The aforementioned experience points to the BGT-2 condition as being accurate for $kR > n + 1$. Hence, we may conclude that on-surface implementation of lower-order radiation conditions is inappropriate to problems with low kR and significant high modes. In finite element implementations R has to be very large if k is low. This greatly increases the computational cost. In this section we review analyses of single mode radiation problems with BGT conditions and verify these conclusions. The analyses are then extended to local DtN conditions with analogous conclusions.

4.1. Cylindrical harmonics

The nth cylindrical mode is [45]

$$u = H_n^{(1)}(kr)\cos n\theta. \tag{21}$$

We now derive specific impedances for cylindrical modes, analyze their asymptotic behavior, and present illustrative examples.

4.1.1. Analysis

We first derive the exact specific impedance of the nth cylindrical mode and analyze its asymptotic behavior.

Lemma 4.1.1. *The exact specific impedance of the nth cylindrical mode on the surface of a cylinder of radius R is*

$$z_n^{\mathrm{ex2}} = z_n = \frac{\mathrm{i}H_n^{(1)}(kR)}{H_n^{(1)'}(kR)}. \tag{22}$$

This expression is independent of the angle θ. The symbols z_n^{ex2} refer to (22) in subsequent usage.

Property 4.1.1. *The asymptotic behavior of the exact specific resistance is*

$$\eta_n \sim \begin{cases} \pi\frac{kR}{2}, & n = 0, \\ \frac{4\pi}{(n!)^2}\left(\frac{kR}{2}\right)^{2n+1}, & n \geqslant 1, \end{cases} \quad \text{as } kR \to 0, \tag{23}$$

$$\eta_n \sim 1, \quad n \geqslant 0 \quad \text{as } kR \to \infty, \tag{24}$$

which indicates passivity.

The asymptotic behavior of the exact specific inertia is

$$\mu_n \sim \begin{cases} -\log\left(\frac{kR}{2}\right), & n = 0, \\ \frac{1}{n}, & n \geqslant 1, \end{cases} \quad \text{as } kR \to 0, \tag{25}$$

$$\mu_n \sim \frac{1}{2(kR)^2}, \quad n \geqslant 0 \quad \text{as } kR \to \infty. \tag{26}$$

Proof. First, we use the recurrence formula of Hankel functions [37, (9.1.27)] to rewrite Eq. (22) as follows

$$z_n^{\text{ex2}} = \frac{\mathrm{i}}{n/kR - H_{n+1}^{(1)}(kR)/H_n^{(1)}(kR)}, \quad n \geqslant 0. \tag{27}$$

Additionally, using the asymptotic forms for small arguments of Bessel functions [37, (9.1.7)–(9.1.9)] and the asymptotic behavior as $kR \to \infty$ [37, (9.2.7), (9.2.9), and (9.2.10)], we deduce that

$$H_n^{(1)}(kR) \sim \begin{cases} 1 + \mathrm{i}\frac{2}{\pi}\log\left(\frac{kR}{2}\right), & n = 0, \\ \frac{1}{n!}\left(\frac{kR}{2}\right)^n - \mathrm{i}\frac{(n-1)!}{\pi}\left(\frac{2}{kR}\right)^n, & n \geqslant 1, \end{cases} \quad \text{as } kR \to 0, \tag{28}$$

$$H_n^{(1)}(kR) \sim \sqrt{\frac{2}{\pi kR}}\left(1 + \mathrm{i}\frac{4n^2-1}{8kR}\right)\exp\left(\mathrm{i}\left(kR - \frac{n\pi}{2} - \frac{\pi}{4}\right)\right), \quad n \geqslant 0 \quad \text{as } kR \to \infty. \tag{29}$$

The asymptotic behavior of the exact specific impedance (22) for small arguments is thus

$$z_n^{\text{ex2}} \sim \begin{cases} \pi\frac{kR}{2} + \mathrm{i}kR\log\left(\frac{kR}{2}\right), & n = 0, \\ \frac{4\pi}{(n!)^2}\left(\frac{kR}{2}\right)^{2n+1} - \mathrm{i}\frac{kR}{n}, & n \geqslant 1, \end{cases} \quad \text{as } kR \to 0. \tag{30}$$

For large arguments

$$\frac{H_{n+1}^{(1)}(kR)}{H_n^{(1)}(kR)} \sim \frac{n+1/2}{kR} - \mathrm{i} \quad \text{as } kR \to \infty, \tag{31}$$

so that

$$z_n^{\text{ex2}} \sim \frac{\mathrm{i}}{n/(kR) - (n+1/2)/(kR) + \mathrm{i}} = \frac{\mathrm{i}}{\mathrm{i} - 1/(2kR)} \quad \text{as } kR \to \infty, \tag{32}$$

and finally

$$z_n^{\text{ex2}} \sim 1 - \frac{\mathrm{i}}{2kR} \quad \text{as } kR \to \infty. \tag{33}$$

Therefore, Property 4.1.1 is an immediate consequence. (Note that the asymptotic behavior for large arguments is independent of mode number n.) □

We now derive specific impedances for cylindrical modes with the local absorbing boundary conditions and analyze their asymptotic behavior.

Lemma 4.1.2. *The* BGT-1 *approximate specific impedance is*

$$z = z_n = \frac{2kR}{2kR + \mathrm{i}}. \tag{34}$$

This result is a direct consequence of using (5) with (21). This expression depends on kR only.

Property 4.1.2. *The asymptotic behavior of the* BGT-1 *specific resistance is*

$$\eta_n \sim (2kR)^2 \quad \text{as } kR \to 0, \tag{35}$$

$$\eta_n \sim 1 \quad \text{as } kR \to \infty, \tag{36}$$

which is passive, as for the exact representation.

The asymptotic behavior of the BGT-1 *specific inertia is*

$$\mu_n \sim 2 \quad \text{as } kR \to 0, \tag{37}$$

$$\mu_n \sim \frac{1}{2(kR)^2} \quad \text{as } kR \to \infty. \tag{38}$$

Proof. These properties result from rewriting Eq. (34) as follows

$$z_n = \frac{4(kR)^2}{4(kR)^2+1} - \mathrm{i}\frac{2kR}{4(kR)^2+1}. \tag{39}$$

It follows that the asymptotic behavior of the BGT-1 specific impedance (34) is

$$z_n \sim (2kR)^2 - 2\mathrm{i}kR \quad \text{as } kR \to 0, \tag{40}$$

$$z_n \sim 1 - \mathrm{i}\frac{1}{2kR} \quad \text{as } kR \to \infty. \tag{41}$$

Therefore, Property 4.1.2 is an immediate consequence. □

The asymptotic behavior of BGT-1 for cylindrical harmonics can be evaluated by comparing (35)–(38) to (23)–(26). The performance at the high wave number limit is *exact*. However, there is loss of accuracy at low wave numbers, particularly for the specific inertia, μ, at higher modes (compare Eq. (37) with (25)).

Lemma 4.1.3. *The* BGT-2 *approximate specific impedance is*

$$z_n = \frac{(kR)^2 + \mathrm{i}kR}{(kR)^2 - 3/8 - n^2/2 + 3\mathrm{i}kR/2}. \tag{42}$$

This result is a direct consequence of using (6) with (21). This expression depends on n, in addition to kR.

Property 4.1.3. *The asymptotic behavior of the* BGT-2 *specific resistance is*

$$\eta_n \sim \frac{8(9-4n^2)}{(3+4n^2)^2}(kR)^2 \quad \text{as } kR \to 0, \tag{43}$$

$$\eta_n \sim 1 \quad \text{as } kR \to \infty. \tag{44}$$

Passivity is lost for $n \geqslant 2$.

The asymptotic behavior of the BGT-2 *specific inertia is*

$$\mu_n \sim \frac{8}{3+4n^2} \quad \text{as } kR \to 0, \tag{45}$$

$$\mu_n \sim \frac{1}{2(kR)^2} \quad \text{as } kR \to \infty. \tag{46}$$

Proof. From Eq. (42), we deduce that

$$\operatorname{Re} z_n = \frac{(kR)^2((kR)^2 + \frac{9}{8} - \frac{n^2}{2})}{(kR)^4 + (\frac{3}{2} - n^2)(kR)^2 + (\frac{n^2}{2} + \frac{3}{8})^2}, \tag{47}$$

and

$$\operatorname{Im} z_n = -\frac{kR(\frac{(kR)^2}{2} + \frac{3}{8} + \frac{n^2}{2})}{(kR)^4 + (\frac{3}{2} - n^2)(kR)^2 + (\frac{n^2}{2} + \frac{3}{8})^2}. \tag{48}$$

It follows that the asymptotic behavior of the BGT-2 specific impedance (42) is

$$z_n \sim \frac{8kR}{3+4n^2}\left(\frac{9-4n^2}{3+4n^2}kR - \mathrm{i}\right) \quad \text{as } kR \to 0, \tag{49}$$

$$z_n \sim 1 - \mathrm{i}\frac{1}{2kR} \quad \text{as } kR \to \infty. \tag{50}$$

Therefore, Property 4.1.3 is an immediate consequence. □

The asymptotic behavior of BGT-2 for cylindrical harmonics can be evaluated by comparing (43)–(46) to (23)–(26). The performance at the high wave number limit is exact, as expected. However, there is loss of accuracy at low wave numbers, particularly for the specific inertia, μ_n, at higher modes (compare Eq. (45) with (25)). Indeed, from (22) and (42), we have

Proposition 4.1.1. *The relative error in the specific impedance of* BGT-2 *is*

$$\lim_{kR\to 0} \frac{z_n^{\mathrm{ex2}} - z_n}{z_n^{\mathrm{ex2}}} \sim 1 - \frac{2}{n} \quad \text{as } n \to \infty. \tag{51}$$

Proof. From Eqs. (22) and (42), we obtain that

$$\lim_{kR\to 0} \frac{z_n}{z_n^{\mathrm{ex2}}} = \frac{8n}{3+4n^2}. \tag{52}$$

Therefore,

$$\lim_{kR\to 0}\left(1 - \frac{z_n}{z_n^{\mathrm{ex2}}}\right) = 1 - \frac{8n}{3+4n^2} \sim 1 - \frac{2}{n} \quad \text{as } n \to \infty. \qquad \square \tag{53}$$

This result clearly indicates that BGT-2 underestimates the exact specific impedance of higher modes at low wave numbers.

Lemma 4.1.4. *The* DtN-1 *approximate specific impedance is*

$$z = z_n = z_0^{\mathrm{ex2}}. \tag{54}$$

This result is a direct consequence of using (10) with (21), and comparing to (22). This expression depends on kR only.

Remark 4.1.1. This expression is exact for $n = 0$, which follows from the design of the DtN boundary condition. Therefore, the asymptotic behavior of this expression is identical to that of z_0^{ex2} (see (23)–(26) for $n = 0$). Hence, the performance of DtN-1 at the high wave number limit is exact, as expected. However, there is loss of accuracy at low wave numbers, particularly for the specific inertia, μ, at higher modes.

Lemma 4.1.5. *The* DtN-2 *approximate specific impedance is*

$$z_n = \frac{1}{1/z_0^{\mathrm{ex2}} + n^2(1/z_1^{\mathrm{ex2}} - 1/z_0^{\mathrm{ex2}})}. \tag{55}$$

This result is a direct consequence of using (11) with (21). This expression depends on n, in addition to kR.

Remark 4.1.2. Thus, the specific impedance of DtN-2 is exact for $n = 0$ and 1, which follows from the design of the DtN boundary condition.

Property 4.1.4. *The asymptotic behavior of the* DtN-2 *specific resistance is*

$$\eta_n \sim \begin{cases} \pi\frac{kR}{2}, & n = 0, \\ \frac{\pi}{2n^2}(kR)^3, & n \geqslant 1, \end{cases} \quad \text{as } kR \to 0, \tag{56}$$

$$\eta_n \sim 1 \quad \text{as } kR \to \infty, \tag{57}$$

which is passive, as for the exact representation.

The asymptotic behavior of the DtN-2 *specific inertia is*

$$\mu_n \sim \begin{cases} -\log\left(\frac{kR}{2}\right), & n = 0, \\ \frac{1}{n^2}, & n \geqslant 1, \end{cases} \quad \text{as } kR \to 0, \tag{58}$$

$$\mu_n \sim \frac{1}{2(kR)^2} \quad \text{as } kR \to \infty. \tag{59}$$

Proof. First, we note (see Eq. (55)) that the limit behavior of the DtN-2 specific impedance is exact for $n = 0$ and 1.

For $n \geqslant 2$, we rewrite Eq. (55) as follows

$$z_n = \frac{z_0^{\mathrm{ex2}} z_1^{\mathrm{ex2}}}{z_1^{\mathrm{ex2}} + n^2(z_0^{\mathrm{ex2}} - z_1^{\mathrm{ex2}})}. \tag{60}$$

Moreover, by the asymptotic behavior of the exact specific impedance for small arguments (30) (see Property 4.1.1), we have

$$z_1^{\mathrm{ex2}} + n^2\left(z_0^{\mathrm{ex2}} - z_1^{\mathrm{ex2}}\right) \sim n^2 z_0^{\mathrm{ex2}} \quad \text{as } kR \to 0. \tag{61}$$

Therefore,

$$z_n \sim \frac{z_1^{\mathrm{ex2}}}{n^2} \quad \text{as } kR \to 0. \tag{62}$$

Hence, Property 4.1.4 is an immediate consequence for $kR \to 0$.

Furthermore, from Eq. (55) and the asymptotic behavior of the exact specific impedance for large arguments (32) (see Property 4.1.1), we deduce that

$$z_n \sim z_0^{\mathrm{ex2}} \quad \text{as } kR \to \infty. \tag{63}$$

Hence, we deduce that

$$z_n \sim 1 - \frac{\mathrm{i}}{2kR} \quad \text{as } kR \to \infty. \tag{64}$$

Property 4.1.4 is then an immediate consequence for $kR \to \infty$. □

The asymptotic behavior of DtN-2 for cylindrical harmonics can be evaluated by comparing (56)–(59) to (23)–(26). As in the case of BGT-2, the performance of DtN-2 at the high wave number limit is exact, as expected. However, there is loss of accuracy at low wave numbers, particularly for the specific inertia, μ_n, at higher modes (compare Eq. (58) with (25)). Indeed, we have

Proposition 4.1.2. *The relative error in the specific impedance of* DtN-2 *is*

$$\lim_{kR\to 0} \frac{z_n^{\mathrm{ex2}} - z_n}{z_n^{\mathrm{ex2}}} \sim 1 - \frac{1}{n} \quad \text{as } n \to \infty. \tag{65}$$

Proof. From Eq. (62) (see Property 4.1.4) we obtain

$$\frac{z_n}{z_n^{\mathrm{ex2}}} \sim \frac{z_1^{\mathrm{ex2}}}{n^2 z_n^{\mathrm{ex2}}} \quad \text{as } kR \to 0. \tag{66}$$

Moreover, using Eq. (30) (see Property 4.1.1), we deduce that

$$\frac{z_n}{z_n^{\mathrm{ex2}}} \sim \frac{4\pi(\frac{kR}{2})^3 - \mathrm{i}kR}{n^2[\frac{4\pi}{(n!)^2}(\frac{kR}{2})^{2n+1} - \mathrm{i}kR/n]} \quad \text{as } kR \to 0. \tag{67}$$

It follows that

$$\lim_{kR\to 0} \frac{z_n}{z_n^{\mathrm{ex2}}} \sim \frac{1}{n} \quad \text{as } n \to \infty, \tag{68}$$

which concludes the proof of Proposition 4.1.2. □

This result clearly indicates that DtN-2 underestimates the exact specific impedance of higher modes at low wave numbers.

4.1.2. Illustrative examples

Figs. 3–6 show the dependence of specific impedance on kR. The limit behavior, as specified above, is easy to verify from the figures. The performance at high wave numbers is accurate, as expected. There is an overall deterioration at low wave numbers. Perhaps surprisingly, BGT is more accurate than

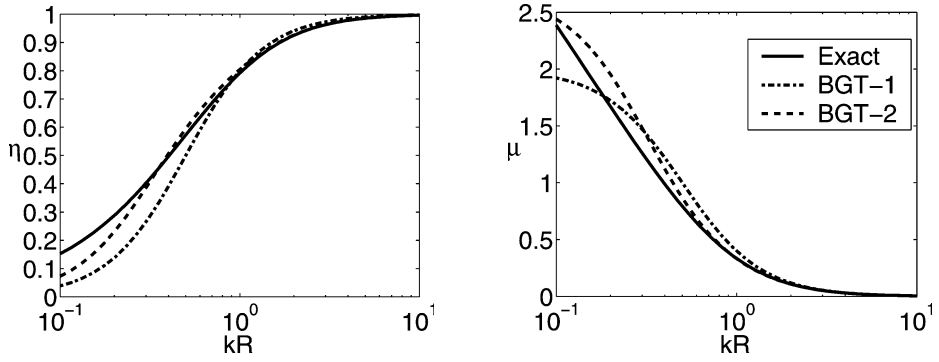

Fig. 3. Specific resistance (left) and inertia (right): cylindrical mode ($n =$) 0; DtN-1 and DtN-2 are exact.

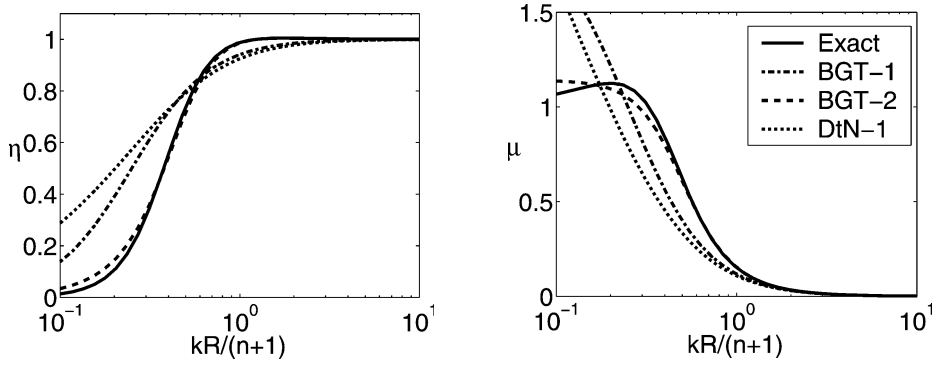

Fig. 4. Specific resistance (left) and inertia (right): cylindrical mode ($n =$) 1; DtN-2 is exact.

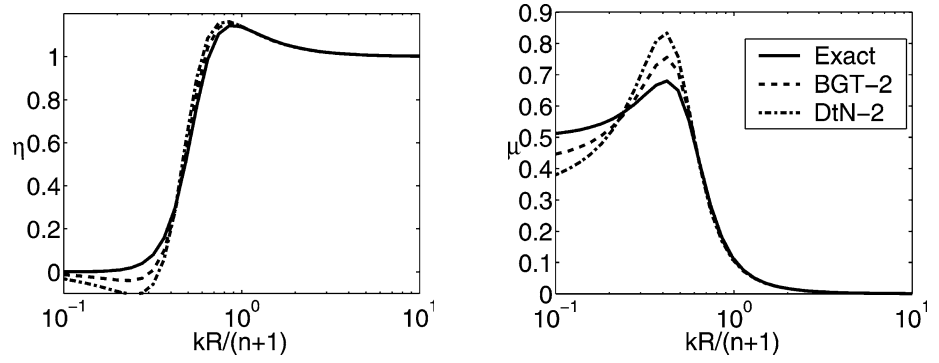

Fig. 5. Specific resistance (left) and inertia (right): cylindrical mode ($n =$) 2.

DtN for low wave numbers in Figs. 4–6, while both approaches contain errors as a result of truncated operators, BGT in two dimensions is based on high kR asymptotics, introducing another source of error. The numerical results in Figs. 4–6 seem to indicate that these two sources of error offset each other to a certain extent.

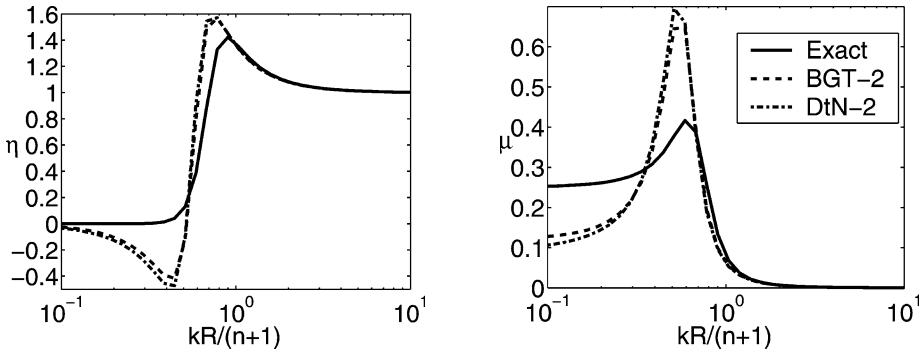

Fig. 6. Specific resistance (left) and inertia (right): cylindrical mode ($n =$) 4.

Both BGT-2 and DtN-2 underestimate exact values, particularly of specific inertia, at very low wave numbers for modes higher than $n = 1$ (Figs. 5 and 6), as predicted. For lower modes ($n = 0$ and 1) BGT-1 is accurate at $kR > (n + 1)$. DtN-1 is exact for $n = 0$ and otherwise is similar in performance to BGT-1. Both are accurate for higher modes ($n > 1$, not shown in figures) only at $kR \gg (n + 1)$. DtN-2 is exact for the first two modes ($n = 0$ and 1), and otherwise is similar in performance to BGT-2. Both retain accuracy for all modes at $kR > (n + 1)$. Thus, if n is high and k is low, R must be large for good performance of BGT-2 and DtN-2.

Figs. 5 and 6 reveal that BGT-2 and DtN-2 are not passive for higher cylindrical radiation modes ($n > 1$) at $kR < n + 1$. We note that an investigation of the effect of lack of passivity on the performance of artificial boundary conditions [44] indicates that it need not be deleterious.

4.2. Axisymmetric spherical harmonics

The axisymmetric spherical mode is [45]

$$u = h_n^{(1)}(kr)\,P_n(\cos\phi). \tag{69}$$

Here, $P_n(\cos\phi)$ is the Legendre polynomial, which satisfies the Legendre equation

$$\frac{\mathrm{d}}{\mathrm{d}\phi}\left(\sin\phi\,\frac{\mathrm{d}(P_n(\cos\phi))}{\mathrm{d}\phi}\right) + n(n+1)\sin\phi\,P_n(\cos\phi) = 0. \tag{70}$$

We now derive specific impedances for axisymmetric spherical modes, analyze their asymptotic behavior, and present illustrative examples.

4.2.1. Analysis

We first derive the *exact* specific impedance of the nth axisymmetric spherical mode and analyze its asymptotic behavior.

Lemma 4.2.1. *The exact specific impedance of the nth axisymmetric spherical mode on the surface of a sphere of radius R is*

$$z_n^{\mathrm{ex3}} = z_n = \frac{\mathrm{i}h_n^{(1)}(kR)}{h_n^{(1)'}(kR)}. \tag{71}$$

This expression is independent of the angle ϕ. The symbols z_n^{ex3} refer to (71) in subsequent usage.

Remark 4.2.1. By applying recursion properties of spherical Hankel functions (15) in Eq. (16), and by [37, (10.1.2) and (10.1.3)], one can easily verify that

$$z_0^{\mathrm{ex3}} = \frac{kR}{kR + \mathrm{i}}, \tag{72}$$

$$z_1^{\mathrm{ex3}} = \frac{(kR)^2 + \mathrm{i}kR}{(kR)^2 - 2 + 2\mathrm{i}kR}. \tag{73}$$

Remark 4.2.2. Property 4.2.1 below makes use of the double factorial, defined by [46]

$$n!! = \begin{cases} 1 \cdot 3 \cdot 5 \cdots (n-2)n & n \text{ odd}, \\ 2 \cdot 4 \cdot 6 \cdots (n-2)n & n \text{ even}, \\ 1 & n = -1, 0. \end{cases} \tag{74}$$

Property 4.2.1. *The asymptotic behavior of the exact specific resistance is*

$$\eta_n \sim \begin{cases} \left(\frac{(kR)^{n+1}}{(n+1)(2n-1)!!}\right)^2 & \text{as } kR \to 0, \\ 1 & \text{as } kR \to \infty, \end{cases} \tag{75}$$

which indicates passivity.

The asymptotic behavior of the exact specific inertia is

$$\mu_n \sim \begin{cases} \frac{1}{n+1} & \text{as } kR \to 0, \\ \frac{1}{(kR)^2} & \text{as } kR \to \infty. \end{cases} \tag{76}$$

Proof. First, we use the recurrence formula of spherical Hankel functions (15) to rewrite Eq. (71) as follows

$$z_n^{\mathrm{ex3}} = \frac{\mathrm{i}}{n/kR - h_{n+1}^{(1)}(kR)/h_n^{(1)}(kR)} \quad n \geqslant 0. \tag{77}$$

From the limiting form of spherical Bessel functions for small arguments [37, (10.1.1)–(10.1.5)], we deduce that

$$h_n^{(1)}(kR) \sim \frac{(kR)^n}{(2n+1)!!} - \mathrm{i}\frac{(2n-1)!!}{(kR)^{n+1}} \quad \text{as } kR \to 0. \tag{78}$$

Thus

$$\frac{h_{n+1}^{(1)}(kR)}{h_n^{(1)}(kR)} \sim \frac{2n+1}{kR} - \mathrm{i}\left(\frac{(kR)^n}{(2n-1)!!}\right)^2 \quad \text{as } kR \to 0, \tag{79}$$

so that

$$z_n^{\mathrm{ex3}} \sim \frac{\mathrm{i}}{n/(kR) - (2n+1)/(kR) + \mathrm{i}((kR)^n/(2n-1)!!)^2} \quad \text{as } kR \to 0, \tag{80}$$

and finally

$$z_n^{\mathrm{ex3}} \sim \left(\frac{(kR)^{n+1}}{(n+1)(2n-1)!!}\right)^2 - \frac{\mathrm{i}kR}{n+1} \quad \text{as } kR \to 0. \tag{81}$$

Therefore, the limits for small arguments in Property 4.2.1 are an immediate consequence.

From the limiting form of spherical Bessel functions for large arguments [37, (10.1.8)–(10.1.9)], we deduce that

$$h_n^{(1)}(kR) \sim \frac{(-1)^n}{kR}\left(\frac{n(n+1)}{2kR} - \mathrm{i}\right)\exp\left(\mathrm{i}\left(kR + \frac{n\pi}{2}\right)\right) \quad \text{as } kR \to \infty. \tag{82}$$

Thus

$$\frac{h_{n+1}^{(1)}(kR)}{h_n^{(1)}(kR)} \sim -\mathrm{i} + \frac{n+1}{kR} \quad \text{as } kR \to \infty, \tag{83}$$

so that

$$z_n^{\mathrm{ex3}} \sim \frac{\mathrm{i}}{n/(kR) + \mathrm{i} - (n+1)/(kR)} \sim 1 - \frac{\mathrm{i}}{kR} \quad \text{as } kR \to \infty, \tag{84}$$

which concludes the proof of Property 4.2.1 in the limit for large arguments. (Note that the asymptotic behavior for large arguments is independent of mode number n.) □

We now derive specific impedances for axisymmetric spherical modes with the local absorbing boundary conditions and analyze their asymptotic behavior. Recall that in three dimensions, DtN-n are identical to BGT-n for $n = 1, 2$ (see Proposition 3.2.1).

Lemma 4.2.2. *The* BGT/DtN-1 *approximate specific impedance is*

$$z = z_n = z_0^{\mathrm{ex3}}. \tag{85}$$

This result is a direct consequence of using (7) or (12) with (69) in (17), and comparing to (71). This expression depends on kR only.

Remark 4.2.3. This expression is exact for $n = 0$, which follows from the design of the BGT and DtN boundary conditions. Therefore, the limit behavior of this expression is identical to that of z_0^{ex3} (see (75)–(76) for $n = 0$). Hence, the performance of BGT/DtN-1 at the high wave number limit is correct, as expected. Still, there is loss of accuracy at low wave numbers, particularly for the specific inertia, μ, at higher modes.

Lemma 4.2.3. *The* BGT/DtN-2 *approximate specific impedance is*

$$z_n = \frac{1}{1/z_0^{\mathrm{ex3}} + n(n+1)(1/z_1^{\mathrm{ex3}} - 1/z_0^{\mathrm{ex3}})/2}. \tag{86}$$

This result is a direct consequence of using (8) or (13), and (70), with (69). This expression depends on n, in addition to kR.

Remark 4.2.4. Eq. (86) indicates that the specific impedance of BGT/DtN-2 is exact for $n = 0$ and 1, which follows from the design of the BGT and DtN boundary conditions.

Property 4.2.2. *The asymptotic behavior of the* BGT/DtN-2 *specific resistance is*

$$\eta_n \sim \begin{cases} -2\frac{n(n+1)-2}{(n(n+1)+2)^2}(kR)^2 & \text{as } kR \to 0, \\ 1 & \text{as } kR \to \infty. \end{cases} \tag{87}$$

Passivity is lost for $n \geqslant 2$.

The asymptotic behavior of the BGT/DtN-2 *specific inertia is*

$$\mu_n \sim \begin{cases} \frac{2}{n(n+1)+2} \\ \frac{1}{(kR)^2} \end{cases} \quad \text{as } kR \to \infty. \tag{88}$$

Proof. First, we note that the limit behavior of the BGT/DtN-2 specific impedance (86) is exact for $n = 0$ and 1. For $n \geqslant 2$, we write Eq. (86) as follows

$$z_n = \frac{2z_0^{\text{ex3}} z_1^{\text{ex3}}}{2z_1^{\text{ex3}} + n(n+1)(z_0^{\text{ex3}} - z_1^{\text{ex3}})}. \tag{89}$$

Then, using Eq. (81) for $n = 0$ and 1 (see Property 4.2.1), one can verify that

$$\operatorname{Re} z_n \sim -\frac{(kR)^2(n(n+1)/2 - 1)}{(1 + n(n+1)/2)^2} \quad \text{as } kR \to 0, \tag{90}$$

and

$$\operatorname{Im} z_n \sim -\frac{2kR}{1 + n(n+1)/2} \quad \text{as } kR \to 0. \tag{91}$$

Therefore, the asymptotic behavior, as $kR \to 0$, of the BGT/DtN-2 specific impedance (86) is

$$z_n \sim -2\frac{n(n+1) - 2}{(n(n+1) + 2)^2}(kR)^2 - \mathrm{i}\frac{2kR}{n(n+1) + 2}, \quad n \geqslant 2 \quad \text{as } kR \to 0, \tag{92}$$

which concludes the proof of Property 4.2.2 for $kR \to 0$.

Applying Eq. (84) for $n = 0$ and 1 (see Property 4.2.1) to Eq. (89), we deduce that

$$z_n \sim z_0^{\text{ex3}} \quad \text{as } kR \to \infty. \tag{93}$$

Therefore, the asymptotic behavior, as $kR \to \infty$, of the BGT/DtN-2 specific impedance (86) is

$$z_n \sim 1 - \frac{\mathrm{i}}{kR} \quad n \geqslant 2 \quad \text{as } kR \to \infty, \tag{94}$$

which concludes the proof of Property 4.2.2 for $kR \to \infty$. □

The asymptotic behavior of BGT/DtN-2 for spherical harmonics can be evaluated by comparing (87)–(88) to (75)–(76). Again, the performance at the high wave number limit is correct, as expected. However, there is loss of accuracy at low wave numbers, particularly for the specific inertia, μ_n, at higher modes. Indeed, we have

Proposition 4.2.1. *The relative error in the specific impedance of* BGT/DtN-2 *for* $n \geqslant 2$ *is*

$$\lim_{kR \to 0} \frac{z_n^{\text{ex3}} - z_n}{z_n^{\text{ex3}}} \sim 1 - \frac{2}{n} \quad \text{as } n \to \infty. \tag{95}$$

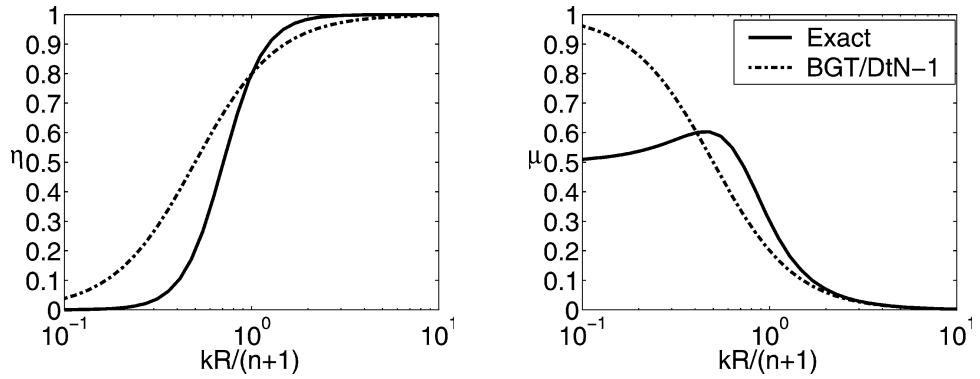

Fig. 7. Specific resistance (left) and inertia (right): Axisymmetric spherical mode ($n =$) 1; BGT/DtN-2 is exact.

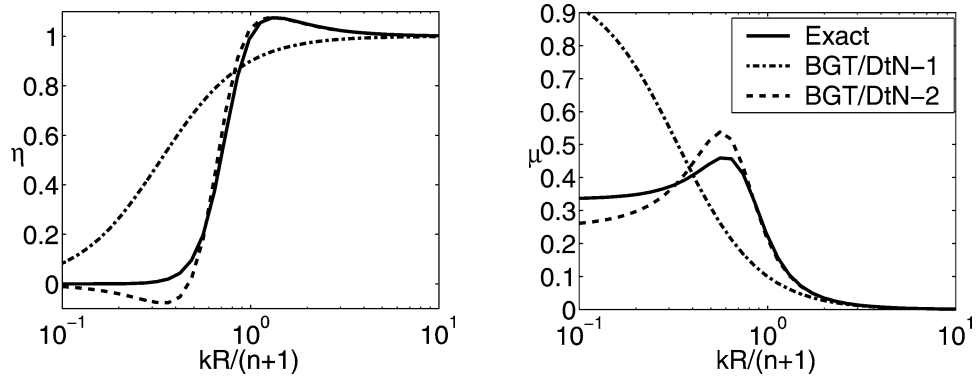

Fig. 8. Specific resistance (left) and inertia (right): Axisymmetric spherical mode ($n =$) 2.

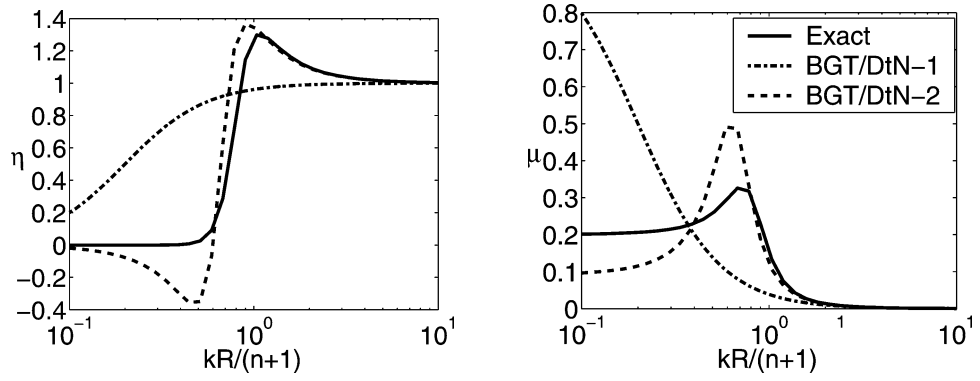

Fig. 9. Specific resistance (left) and inertia (right): Axisymmetric spherical mode ($n =$) 4.

Proof. From Eq. (92) (see Property 4.2.2) and Eq. (81) (see Property 4.2.1), we deduce that

$$\lim_{kR\to 0} \frac{z_n}{z_n^{\mathrm{ex3}}} = \frac{1+n}{1+n(n+1)/2}. \tag{96}$$

Hence,

$$\lim_{kR\to 0}\left(1-\frac{z_n}{z_n^{\mathrm{ex3}}}\right)=\frac{2+(n-1)(n+1)}{2+n(n+1)}. \tag{97}$$

Therefore, Proposition 4.2.1 is proved. □

This result clearly indicates that BGT/DtN-2 underestimates the exact specific impedance of higher modes at low wave numbers.

4.2.2. Illustrative examples

Figs. 7–9 show the dependence of specific impedance on kR. The limit behavior, as specified above, is easy to verify from the figures. The performance at high wave numbers is accurate, as expected. There is an overall deterioration at low wave numbers. BGT/DtN-2 underestimates exact values, particularly of specific inertia, at very low wave numbers for modes higher than $n=1$ (Figs. 8 and 9), as predicted. BGT/DtN-1 is accurate only at $kR \gg (n+1)$, except for the breathing mode ($n=0$), where BGT/DtN-1 (85) is exact and identical to BGT/DtN-2 (86). BGT/DtN-2 is exact for the first two modes ($n=0$ and 1, Fig. 7). BGT/DtN-2 retains accuracy for all modes at $kR > (n+1)$. As in two dimensions, if n is high and k is low, R must be large for good performance of BGT/DtN-2.

Figs. 8 and 9 confirm that BGT/DtN-2 is not passive for higher axisymmetric spherical radiation modes ($n>1$) at $kR < n+1$, as in the cylindrical case.

5. Performance of ABC on round obstacles

In this section we derive the specific impedance of on-surface local absorbing conditions for scattering problems, highlighting its behavior at low kR, and compare it to exact values. Specific impedance now depends on the direction of the incident wave.

5.1. Scattering of a plane wave from a soft circular cylinder

Consider an incident plane wave along the positive x-axis

$$u^{\mathrm{i}}=\exp(\mathrm{i}kx), \tag{98}$$

scattered by an infinite circular cylinder of radius R. The angle to the direction of the incident wave is $\theta=\arctan(y/x)$, so that there is no restriction in this choice of direction. Due to the homogeneous Dirichlet boundary condition on the obstacle ($r=R$), imposed on the total field, the scattered field in polar coordinates satisfies

$$u=-\exp(\mathrm{i}kR\cos\theta) \tag{99}$$

(recall $x=r\cos\theta$). We now derive specific impedances for this scattering problem, analyze their asymptotic behavior, and present illustrative examples.

5.1.1. Analysis

Calculating the exact specific impedance requires the normal derivative on the surface, which is obtained from the series representation of the scattered field [28]

$$u(r,\theta) = -2\sum_{n=0}^{\infty}{}' \mathrm{i}^n \frac{J_n(kR)H_n^{(1)}(kr)}{H_n^{(1)}(kR)}\cos n\theta. \tag{100}$$

The prime on the sum indicates that the first term is halved. The derivative on the surface is

$$\frac{\partial u}{\partial r}(R,\theta) = -2k\sum_{n=0}^{\infty}{}' \mathrm{i}^n \frac{J_n(kR)H_n^{(1)'}(kR)}{H_n^{(1)}(kR)}\cos n\theta. \tag{101}$$

The exact specific impedance of the scattered field on the boundary is then obtained by using Eqs. (99) and (101) in Definition 3.3.1. One can observe that the result depends on kR *and* on the angle (from the incident plane wave) θ. Therefore, we write

$$z = z_\theta(kR), \tag{102}$$

in contrast to single mode radiation (where it depends on kR and n).

Property 5.1.1. *The asymptotic behavior of the exact specific resistance is*

$$\eta_\theta \sim \pi\frac{kR}{2} \quad \text{as } kR \to 0, \tag{103}$$

which indicates passivity.

The asymptotic behavior of the exact specific inertia is

$$\mu_\theta \sim -\log\left(\frac{kR}{2}\right) \quad \text{as } kR \to 0. \tag{104}$$

Proof. First, we rewrite the derivative on the surface (101) using the exact specific impedance of the nth cylindrical mode (22) (see Lemma 4.1.1), as follows

$$\frac{\partial u}{\partial r}(R,\theta) = -2k\sum_{n=0}^{\infty}{}' \mathrm{i}^{n+1} \frac{J_n(kR)}{z_n^{\mathrm{ex2}}}\cos n\theta. \tag{105}$$

Moreover, from the asymptotic form of Bessel functions for small arguments [37, (9.1.7)]

$$J_n(kR) \sim \frac{(kR/2)^n}{n!} \quad \text{as } kR \to 0, \tag{106}$$

and using the asymptotic behavior of the exact specific impedance of the nth cylindrical mode for small arguments (30) (see Property 4.1.1), one can verify that

$$\frac{\partial u}{\partial r}(R,\theta) \sim -\mathrm{i}k\frac{J_0(kR)}{z_0^{\mathrm{ex2}}} \sim -\frac{\mathrm{i}k}{z_0^{\mathrm{ex2}}} \quad \text{as } kR \to 0. \tag{107}$$

Since,

$$u(R,\theta) \sim -1 \quad \text{as } kR \to 0, \tag{108}$$

it follows that the asymptotic behavior of the exact specific impedance of a circular cylinder scattering a plane wave is

$$z_\theta \sim \frac{-\mathrm{i}k}{-\mathrm{i}k/z_0^{\mathrm{ex2}}} \sim z_0^{\mathrm{ex2}} \quad \text{as } kR \to 0. \tag{109}$$

Therefore, Property 5.1.1 is a an immediate consequence. □

Remark 5.1.1. One can easily verify that the BGT-1 approximate specific impedance for scattering of a plane wave from a soft circular cylinder is equal to that of cylindrical harmonics, see Eq. (34). Thus, it is problem independent, lacking the angular dependence of the analytical representation.

Lemma 5.1.1. *The* BGT-2 *approximate specific impedance for this problem satisfies*

$$z_\theta = \frac{(kR)^2 + \mathrm{i}kR}{(kR)^2(2-\sin^2\theta)/2 - 3/8 + \mathrm{i}kR(3-\cos\theta)/2}. \tag{110}$$

This result is obtained directly from using Eqs. (6) and (99) in (17). This expression depends on θ, in addition to kR. Compare to (42) for similarities to and differences from the radiation problem.

Property 5.1.2. *The asymptotic behavior of the* BGT-2 *specific resistance is*

$$\eta_\theta \sim \begin{cases} \frac{8}{9}(kR)^2(9-4\cos\theta) & \text{as } kR \to 0, \\ \frac{2}{2-\sin^2\theta} & \text{as } kR \to \infty, \end{cases} \tag{111}$$

which indicates passivity.

The asymptotic behavior of the BGT-2 *specific inertia is*

$$\mu_\theta \sim \begin{cases} \frac{8}{3} & \text{as } kR \to 0, \\ -\frac{2(\cos\theta-1-\sin^2\theta)}{(2-\sin^2\theta)^2}\frac{1}{(kR)^2} & \text{as } kR \to \infty. \end{cases} \tag{112}$$

Proof. From Eq. (110) (see Lemma 5.1.1), we deduce that

$$z_\theta \sim \frac{8}{9}(kR)^2(9-4\cos\theta) - \mathrm{i}\frac{8}{3}kR \qquad \text{as } kR \to 0, \tag{113}$$

$$z_\theta \sim \frac{2}{2-\sin^2\theta}\left(1 + \frac{\mathrm{i}}{kR}\frac{\cos\theta - 1 - \sin^2\theta}{2-\sin^2\theta}\right) \quad \text{as } kR \to \infty. \tag{114}$$

Property 5.1.2 is then an immediate consequence. □

Remark 5.1.2. One can easily verify that the DtN-1 approximate specific impedance for scattering of a plane wave from a soft circular cylinder is equal to that of cylindrical harmonics, see Eq. (34). Thus, it is problem independent, lacking the angular dependence of the analytical representation.

Lemma 5.1.2. *The* DtN-2 *approximate specific impedance for this problem satisfies*

$$z_\theta = \frac{1}{1/z_0^{\mathrm{ex2}} + kR(kR\sin^2\theta + \mathrm{i}\cos\theta)(1/z_1^{\mathrm{ex2}} - 1/z_0^{\mathrm{ex2}})}. \tag{115}$$

This result is obtained directly from Eqs. (11) and (99). Here, z_n^{ex2} are given by Eq. (22). As in the case of BGT-2, the DtN-2 specific impedance depends on θ, in addition to kR. Compare to (55) for similarities to and differences from the radiation problem.

Property 5.1.3. *The asymptotic behavior of the* DtN-2 *specific resistance is*

$$\eta_\theta \sim \begin{cases} \pi \frac{kR}{2} & \text{as } kR \to 0, \\ \frac{2}{2-\sin^2\theta} & \text{as } kR \to \infty, \end{cases} \tag{116}$$

which indicates passivity.

The asymptotic behavior of the DtN-2 *specific inertia is*

$$\mu_\theta \sim \begin{cases} -\log\left(\frac{kR}{2}\right) & \text{as } kR \to 0, \\ -\frac{2(\cos\theta-1-19\sin^2\theta/64)}{(2-\sin^2\theta)^2}\frac{1}{(kR)^2} & \text{as } kR \to \infty. \end{cases} \tag{117}$$

Proof. First, we rewrite Eq. (115) (see Lemma 5.1.2) as follows

$$z_\theta = \frac{z_0^{\mathrm{ex2}}}{1 + kR(kR\sin^2\theta + \mathrm{i}\cos\theta)(z_0^{\mathrm{ex2}}/z_1^{\mathrm{ex2}} - 1)}. \tag{118}$$

Moreover, from Eq. (30) (see Property 4.1.1), one can verify that

$$kR\left(\frac{z_0^{\mathrm{ex2}}}{z_1^{\mathrm{ex2}}} - 1\right) \sim z_0^{\mathrm{ex2}} \quad \text{as } kR \to 0. \tag{119}$$

Hence, it follows from Eq. (118) that the asymptotic behavior, as $kR \to 0$, of the DtN-2 specific impedance (115) is identical to that of the exact specific impedance (109), namely

$$z_\theta \sim z_0^{\mathrm{ex2}} \quad \text{as } kR \to 0, \tag{120}$$

and therefore, Property 5.1.3 is an immediate consequence for $kR \to 0$.

We now prove Property 5.1.3 in the case where $kR \to \infty$. From Eq. (22) (See Lemma 4.1.1) and the recurrence formula [37, (9.1.27)], we have

$$\frac{1}{z_1^{\mathrm{ex2}}} - \frac{1}{z_0^{\mathrm{ex2}}} = \frac{\mathrm{i}}{kR} - \mathrm{i}\left(\frac{H_0^{(1)}(kR)}{H_1^{(1)}(kR)} + \frac{H_1^{(1)}(kR)}{H_0^{(1)}(kR)}\right). \tag{121}$$

Hence, based on the expansion formula of the Hankel functions for large argument [37, (9.2.7)], we have

$$\frac{H_1^{(1)}(kR)}{H_0^{(1)}(kR)} \sim -\mathrm{i}\frac{1 + 3\mathrm{i}/(8kR) + 15/(2(8kR)^2)}{1 - \mathrm{i}/(8kR) - 9/(2(8kR)^2)} \quad \text{as } kR \to \infty. \tag{122}$$

Thus, one can verify that the asymptotic behavior, as $kR \to \infty$, of the DtN-2 specific impedance (115) is

$$z_\theta \sim \frac{2}{2-\sin^2\theta}\left(1 + \frac{\mathrm{i}}{kR}\frac{\cos\theta - 1 - 19\sin^2\theta/64}{2-\sin^2\theta}\right) \quad \text{as } kR \to \infty. \tag{123}$$

which concludes the proof of Property 5.1.3 for $kR \to \infty$. □

Remark 5.1.3. The behavior of the DtN-2 specific impedance at the low wave number limit is identical to the exact cylindrical breathing mode (see Eqs. (23), (25) and (30), for $n = 0$) and DtN-1. For high wave numbers the asymptotic behavior of DtN-2 is similar to BGT-2, as expected, see Eqs. (111), (112), and (114).

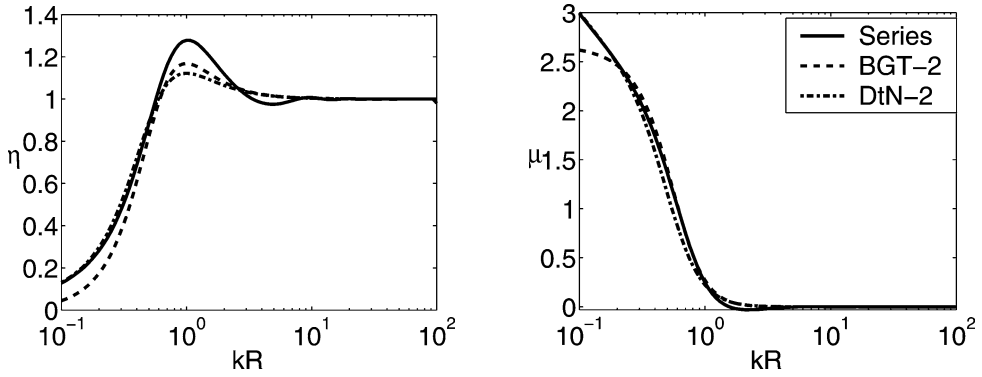

Fig. 10. Specific resistance (left) and inertia (right) at $\theta = 0$: Scattering of a plane wave from a soft circular cylinder.

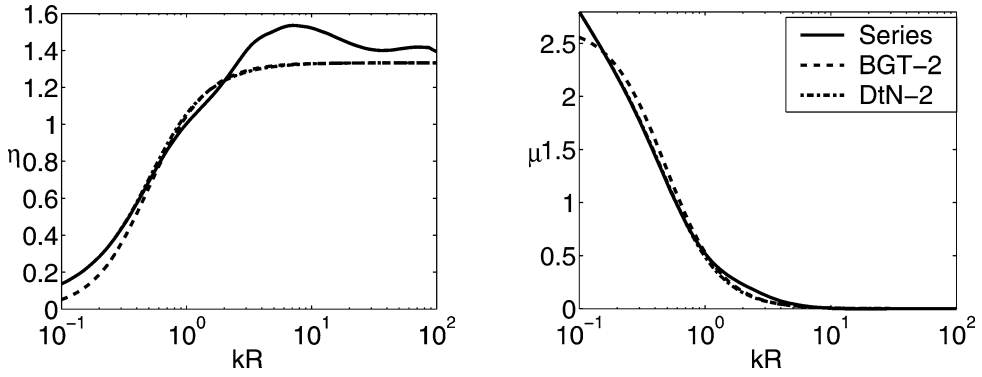

Fig. 11. Specific resistance (left) and inertia (right) at $\theta = \pi/4$: Scattering of a plane wave from a soft circular cylinder.

5.1.2. Illustrative examples

Figs. 10–13 show the components of specific impedance at various angles. There is a large variation in the accuracy at a given kR, but the limit behavior, as specified above, is easy to verify from the figures. BGT-2 and DtN-2 are very similar at large kR. However, the superior performance of DtN-2 over BGT-2 at $kR < 0.5$ is evident. In contrast to the performance for radiation problems, here the boundary conditions exhibit passivity for all cases.

Figs. 14 and 15 show polar plots of the magnitude of the specific impedance. In the very low range ($kR = 0.1$), see Fig. 14, BGT-2 is not accurate, since it is based on high kR asymptotic representations of $H_n^{(1)}(kR)$. On the other hand, DtN-2 is indistinguishable in this case from the series solution. The situation for BGT-2 improves in the middle range ($kR = 1$ and 10). In the higher range ($kR = 100$) there is a loss of accuracy for both BGT-2 and DtN-2. OSRC implementation of the ABCs is inappropriate for scattering problems at high kR, as previously observed [23]. This is not a concern for implementation on an artificial boundary. The important observation in this case is that BGT-2 is accurate for this scattering problem at wave numbers as low as $kR = 1$ (and even somewhat lower), and DtN-2 exhibits very high accuracy at wave numbers as low as $kR = 0.1$, in contrast to experience from radiation problems.

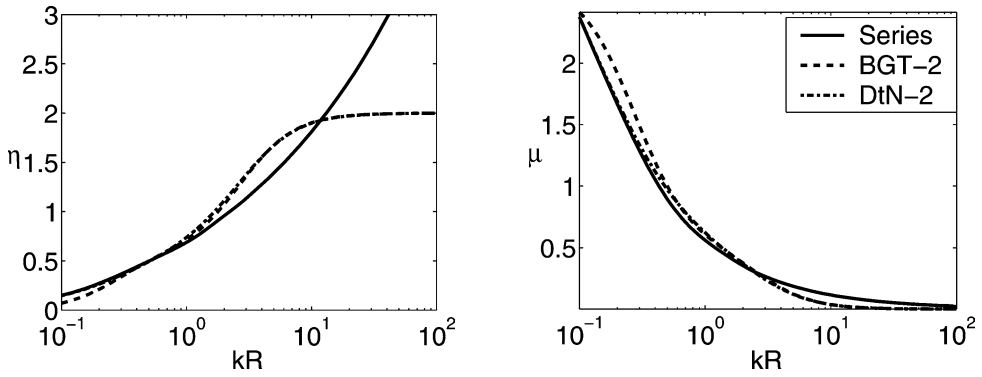

Fig. 12. Specific resistance (left) and inertia (right) at $\theta = \pi/2$: Scattering of a plane wave from a soft circular cylinder.

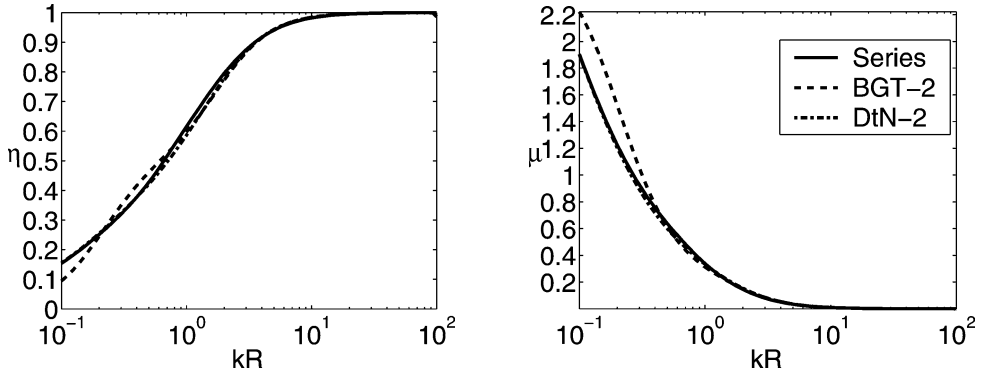

Fig. 13. Specific resistance (left) and inertia (right) at $\theta = \pi$: Scattering of a plane wave from a soft circular cylinder.

5.2. *Scattering of a plane wave from a soft sphere*

Consider an incident plane wave along the positive z-axis (not to be confused with specific impedance)

$$u^{\mathrm{i}} = \exp(\mathrm{i}kz), \tag{124}$$

scattered by a sphere of radius R. The angle to the direction of the incident wave is $\phi = \arctan(\sqrt{x^2 + y^2}/z)$, so that there is no restriction in this choice of direction. Due to the homogeneous Dirichlet boundary condition on the obstacle ($r = R$), imposed on the total field, the scattered field in spherical coordinates is

$$u = -\exp(\mathrm{i}kR\cos\phi) \tag{125}$$

(recall $z = r\cos\phi$). We now derive specific impedances for this scattering problem, analyze their asymptotic behavior, and present illustrative examples.

5.2.1. *Analysis*

Calculating the exact specific impedance requires the normal derivative on the surface, which is obtained from the series representation of the scattered field [28]

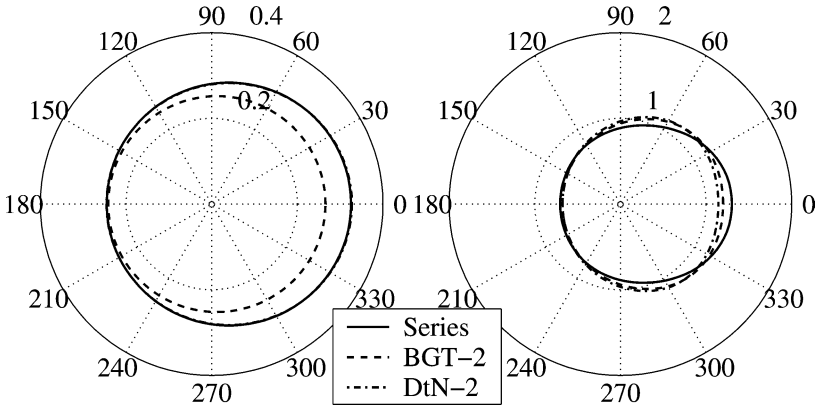

Fig. 14. Magnitude of specific impedance, $kR = 0.1$ (left) and $kR = 1$ (right): Scattering of a plane wave from a soft circular cylinder.

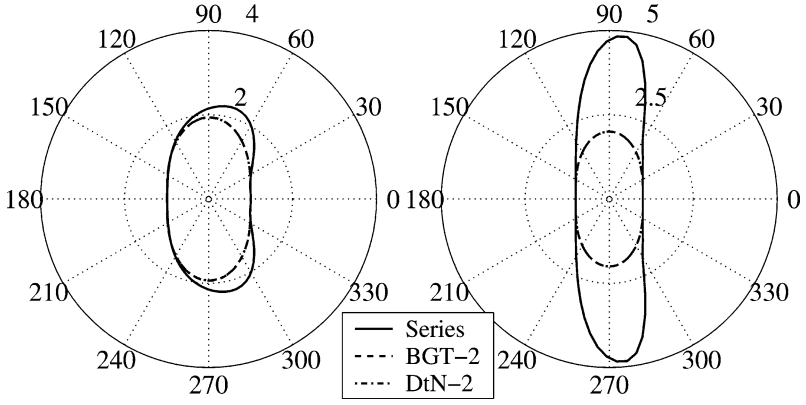

Fig. 15. Magnitude of specific impedance, $kR = 10$ (left) and $kR = 100$ (right): Scattering of a plane wave from a soft circular cylinder.

$$u(r,\theta,\phi) = -\sum_{n=0}^{\infty} \mathrm{i}^n (2n+1) \frac{j_n(kR) h_n^{(1)}(kr)}{h_n^{(1)}(kR)} P_n(\cos\phi). \tag{126}$$

The derivative on the surface is

$$\frac{\partial u}{\partial r}(R,\theta,\phi) = -k \sum_{n=0}^{\infty} \mathrm{i}^n (2n+1) \frac{j_n(kR) h_n^{(1)'}(kR)}{h_n^{(1)}(kR)} P_n(\cos\phi). \tag{127}$$

The exact specific impedance of the scattered field on the boundary is obtained by using Eqs. (125) and (127) in Definition 3.3.1. One can observe that the result depends on kR *and* on the angle (from the incident plane wave) ϕ. Therefore, we write

$$z = z_\phi(kR), \tag{128}$$

in contrast to single mode radiation (where it depends on kR and n).

Property 5.2.1. *The asymptotic behavior of the exact specific resistance is*

$$\eta_\phi \sim (kR)^2 \quad \text{as } kR \to 0, \tag{129}$$

which indicates passivity.

The asymptotic behavior of the exact specific inertia is

$$\mu_\phi \sim 1 \quad \text{as } kR \to 0. \tag{130}$$

Proof. First, we rewrite the derivative on the surface (127) using the exact specific impedance of the nth axisymmetric spherical mode (71) (see Lemma 4.2.1), as follows

$$\frac{\partial u}{\partial r}(R,\theta,\phi) = -k \sum_{n=0}^{\infty} \mathrm{i}^{n+1}(2n+1)\frac{j_n(kR)}{z_n^{\mathrm{ex3}}} P_n(\cos\phi). \tag{131}$$

Moreover, from the limiting form of spherical Bessel functions for small arguments [37, (10.1.2)]

$$j_n(kR) \sim \frac{(kR)^n}{(2n+1)!!} \quad \text{as } kR \to 0, \tag{132}$$

and using the asymptotic behavior of the exact specific impedance of the nth axisymmetric spherical mode for small arguments (81) (see Property 4.2.1), one can verify that

$$\frac{\partial u}{\partial r}(R,\theta,\phi) \sim -\mathrm{i}k\frac{j_0(kR)}{z_0^{\mathrm{ex3}}} \sim -\frac{\mathrm{i}k}{z_0^{\mathrm{ex3}}} \quad \text{as } kR \to 0. \tag{133}$$

Since,

$$u(R,\theta,\phi) \sim -1 \quad \text{as } kR \to 0, \tag{134}$$

it follows that the asymptotic behavior of the exact specific impedance of a sphere scattering a plane wave is

$$z_\phi \sim \frac{-\mathrm{i}k}{-\mathrm{i}k/z_0^{\mathrm{ex3}}} \sim z_0^{\mathrm{ex3}} \quad \text{as } kR \to 0. \tag{135}$$

Therefore, Property 5.2.1 is a an immediate consequence. □

Remark 5.2.1. The BGT/DtN-1 approximate specific impedance is problem independent, see Eq. (85), lacking the angular dependence of the analytical representation.

Lemma 5.2.1. *The* BGT/DtN-2 *approximate specific impedance for this problem satisfies*

$$z_\phi = \frac{1}{1/z_0^{\mathrm{ex3}} + kR(kR\sin^2\phi + 2\mathrm{i}\cos\phi)(1/z_1^{\mathrm{ex3}} - 1/z_0^{\mathrm{ex3}})/2}. \tag{136}$$

This result is obtained directly from Eqs. (8) and (13), and (125) (assuming no longitudinal dependence). Here, z_n^{ex3} are given by Eq. (71). The approximate BGT/DtN-2 specific impedance for this case depends on ϕ, in addition to kR. Compare to (86) for similarities to and differences from the radiation problem.

Property 5.2.2. *The asymptotic behavior of the* BGT/DtN-2 *specific resistance is*

$$\eta_\phi \sim \begin{cases} (1-\cos\phi)(kR)^2 & \text{as } kR \to 0, \\ \frac{2}{2-\sin^2\phi} & \text{as } kR \to \infty, \end{cases} \tag{137}$$

which indicates passivity.

The asymptotic behavior of the BGT/DtN-2 *specific inertia is*

$$\mu_\phi \sim \begin{cases} 1 & \text{as } kR \to 0, \\ -\frac{2(2\cos\phi-2-\sin^2\phi)}{(2-\sin^2\phi)^2}\frac{1}{(kR)^2} & \text{as } kR \to \infty. \end{cases} \tag{138}$$

Proof. Substituting the explicit expressions for the exact specific impedance of the first two axisymmetric spherical modes (72) and (73) into the BGT/DtN-2 approximate specific impedance for the scattering of a plane wave from a soft sphere (136), we obtain

$$z_\phi = \frac{(kR)^2 + \mathrm{i}kR}{(kR)^2(2-\sin^2\phi)/2 - 1 + \mathrm{i}kR(2-\cos\phi)}. \tag{139}$$

The asymptotic behavior is thus

$$z_\phi \sim (1-\cos\phi)(kR)^2 - \mathrm{i}kR \qquad \text{as } kR \to 0, \tag{140}$$

$$z_\phi \sim \frac{2}{2-\sin^2\phi}\left(1 + \frac{\mathrm{i}}{kR}\frac{2\cos\phi - 2 - \sin^2\phi}{2-\sin^2\phi}\right) \qquad \text{as } kR \to \infty. \tag{141}$$

Property 5.2.2 is then an immediate consequence. □

Remark 5.2.2. The behavior of the BGT/DtN-2 approximate specific impedance for the scattering of a plane wave from a soft sphere at the low wave number limit is similar to the exact spherical breathing mode (see (81) for $n = 0$) and BGT/DtN-1. For high wave numbers the asymptotic behavior of BGT/DtN-2 specific resistance is identical to the two-dimensional case.

5.2.2. Illustrative examples

Figs. 16–19 show the components of specific impedance at various angles. There is a large variation in the accuracy at a given kR, but the limit behavior, as specified above, is easy to verify from the figures.

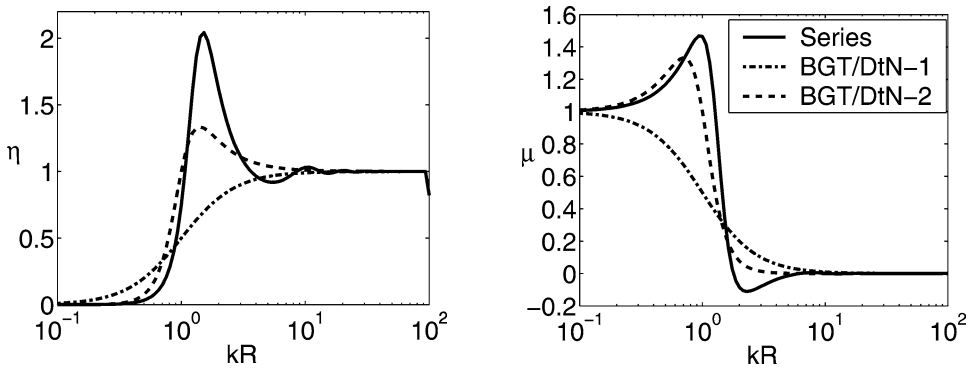

Fig. 16. Specific resistance (left) and inertia (right) at $\phi = 0$: Scattering of a plane wave from a soft sphere.

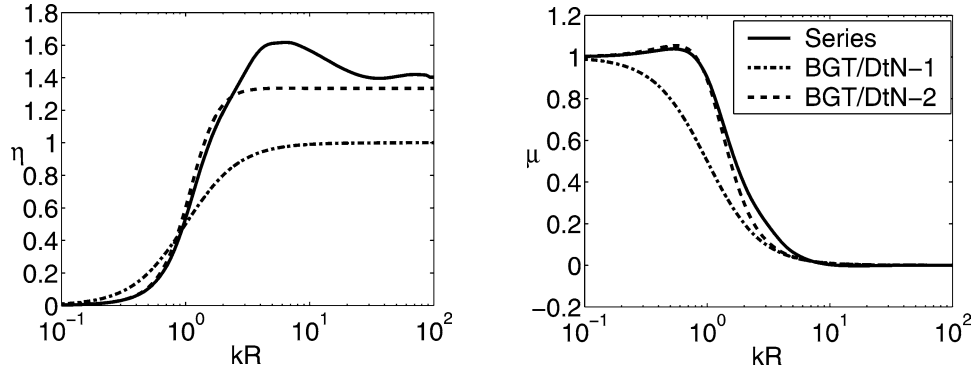

Fig. 17. Specific resistance (left) and inertia (right) at $\phi = \pi/4$: Scattering of a plane wave from a soft sphere.

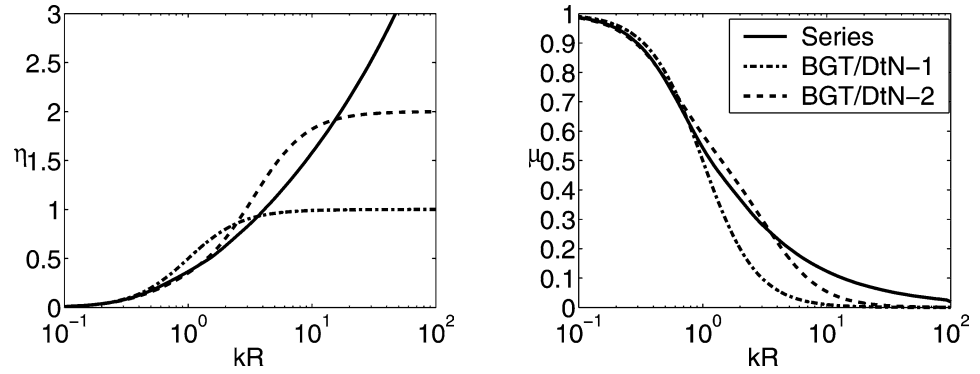

Fig. 18. Specific resistance (left) and inertia (right) at $\phi = \pi/2$: Scattering of a plane wave from a soft sphere.

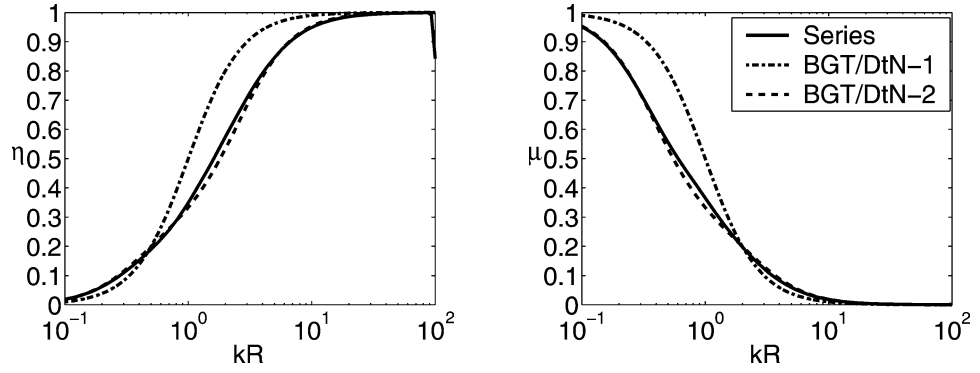

Fig. 19. Specific resistance (left) and inertia (right) at $\phi = \pi$: Scattering of a plane wave from a soft sphere.

As in the case of scattering from a cylinder, and in contrast to the performance for radiation problems, here the boundary conditions exhibit passivity for all cases.

Figs. 20 and 21 show polar plots of the magnitude of the specific impedance. The false isotropy of BGT/DtN-1 is evident. BGT/DtN-2 is accurate in the lower to middle range ($0.1 < kR < 10$). The accuracy in the low range ($kR < 0.1$) is better than BGT2 in two dimensions. As in two dimensions,

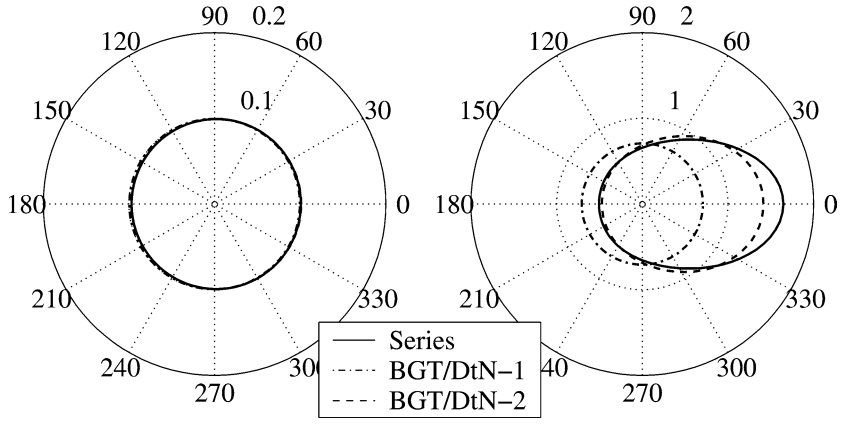

Fig. 20. Magnitude of specific impedance, $kR = 0.1$ (left) and $kR = 1$ (right): Scattering of a plane wave from a soft sphere.

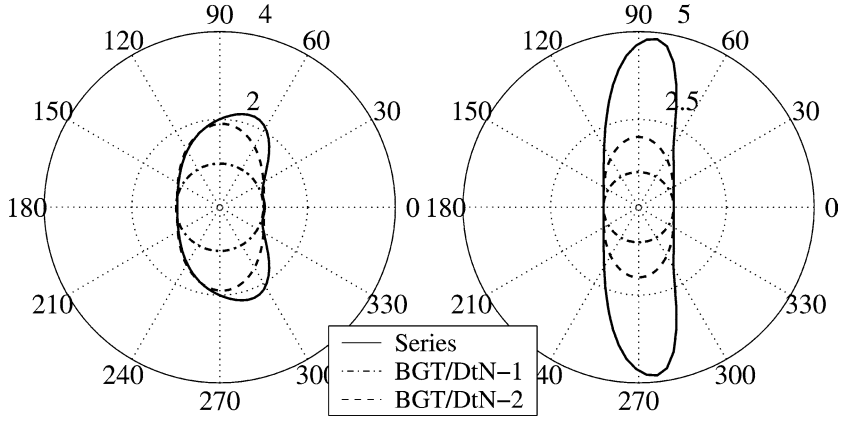

Fig. 21. Magnitude of specific impedance, $kR = 10$ (left) and $kR = 100$ (right): Scattering of a plane wave from a soft sphere.

there is deterioration in the higher range ($kR = 100$). Again, we see that OSRC implementation of the BGT/DtN condition is inappropriate for scattering problems at high kR, as also observed in [23]. This is not a concern for implementation on an artificial boundary. As before, the important observation in this case is that BGT/DtN-2 is accurate for this scattering problem at wave numbers lower than $kR = 1$, in contrast to experience from radiation problems.

6. Summary and conclusions

In this paper, we analyze the effect of wave number, specifically kR, on the performance of BGT and local DtN absorbing boundary conditions. The boundary conditions in the analyses are specified on simple shapes as on-surface radiation conditions. Performance is measured by comparing approximate and exact specific acoustic impedances.

A review of single mode cylindrical and spherical *radiation* confirms the conclusion that the BGT-2 and DtN-2 conditions are accurate for $kR > n + 1$, where n is the mode number, potentially rendering

OSRC implementation inappropriate in the presence of significant high modes, and increasing the computational cost of finite element implementation.

A similar analysis of plane wave *scattering* by a cylinder and a sphere indicates that the range of satisfactory performance on scattering problems extends to relatively low kR. In two dimensions BGT-2 deteriorates at very low kR (since it is based on high kR-asymptotic representations of Hankel functions), but DtN-2 retains its excellent performance. Superior performance at very low kR is exhibited by BGT/DtN-2 in three dimensions. This result is expected, since it merely states that high modes are less significant at low wave numbers. The analysis shows that it applies to problems with approximate boundary conditions as well exact representations. Furthermore, we are able to quantify this effect, providing guidelines for practical computation. The guidelines indicate that relatively small computational domains can be employed in most practical applications for the simple cylindrical and spherical geometries considered, in order to avoid excessive computational cost.

We plan to address other measures of performance, as well as radiation and scattering from elongated geometries in future research.

Acknowledgements

The authors wish to thank Xavier Antoine, Jeremy Astley, Jeff Cipolla, Charbel Farhat, Tom Geers, Dan Givoli, Marcus Grote, and Eli Turkel for helpful discussions. The second author was supported by the Office of Naval Research, under grant N-00014-95-1-0663.

References

[1] D. Givoli, Numerical Methods For Problems in Infinite Domains, Stud. Appl. Mech., vol. 33, Elsevier, Amsterdam, 1992.
[2] R.J. Astley, Mapped spheroidal wave-envelope elements for unbounded wave problems, Internat. J. Numer. Methods Engrg. 41 (7) (1998) 1235–1254.
[3] P. Bettess, Infinite Elements, Penshaw Press, Sunderland, 1992.
[4] D.S. Burnett, R.L. Holford, An ellipsoidal acoustic infinite element, Comput. Methods Appl. Mech. Engrg. 164 (1–2) (1998) 49–76.
[5] J.L. Cipolla, M.J. Butler, Infinite elements in the time domain using a prolate spheroidal multipole expansion, Internat. J. Numer. Methods Engrg. 43 (5) (1998) 889–908.
[6] I. Harari, P. Barai, P.E. Barbone, Numerical and spectral investigations of Trefftz infinite elements, Internat. J. Numer. Methods Engrg. 46 (4) (1999) 553–577.
[7] H.S. Chen, C.C. Mei, Oscillations and wave forces in a man-made harbor in the open sea, in: Tenth Symposium on Naval Hydrodynamics, Office of Naval Research, Department of the Navy, Cambridge, MA, 1974, pp. 573–594.
[8] M.J. Grote, J.B. Keller, Nonreflecting boundary conditions for time-dependent scattering, J. Comput. Phys. 127 (1) (1996) 52–65.
[9] B. Gustafsson, H.-O. Kreiss, Boundary conditions for time-dependent problems with an artificial boundary, J. Comput. Phys. 30 (3) (1979) 333–351.
[10] T. Hagstrom, H.B. Keller, Exact boundary conditions at an artificial boundary for partial differential equations in cylinders, SIAM J. Math. Anal. 17 (2) (1986) 322–341.
[11] D. Givoli, Exact representations on artificial interfaces and applications in mechanics, AMR 52 (11) (1999) 333–349.
[12] X. Antoine, H. Barucq, A. Bendali, Bayliss–Turkel-like radiation conditions on surfaces of arbitrary shape, J. Math. Anal. Appl. 229 (1) (1999) 184–211.
[13] A. Bayliss, M. Gunzburger, E. Turkel, Boundary conditions for the numerical solution of elliptic equations in exterior regions, SIAM J. Appl. Math. 42 (2) (1982) 430–451.

[14] B. Engquist, A. Majda, Absorbing boundary conditions for the numerical simulation of waves, Math. Comp. 31 (139) (1977) 629–652.
[15] D. Givoli, I. Patlashenko, J.B. Keller, High-order boundary conditions and finite elements for infinite domains, Comput. Methods Appl. Mech. Engrg. 143 (1–2) (1997) 13–39.
[16] S. Jones, Douglas, Surface radiation conditions, IMA J. Appl. Math. 41 (1) (1988) 21–30.
[17] A.J. Safjan, Highly accurate non-reflecting boundary conditions for finite element simulations of transient acoustics problems, Comput. Methods Appl. Mech. Engrg. 152 (1–2) (1998) 175–193.
[18] D. Givoli, J.B. Keller, Nonreflecting boundary conditions for elastic waves, Wave Motion 12 (3) (1990) 261–279.
[19] R. Djellouli, C. Farhat, A. Macedo, R. Tezaur, Finite element solution of two-dimensional acoustic scattering problems using arbitrarily shaped convex artificial boundaries, J. Comput. Acoust. 8 (1) (2000) 81–99.
[20] J.J. Shirron, I. Babuška, A comparison of approximate boundary conditions and infinite element methods for exterior Helmholtz problems, Comput. Methods Appl. Mech. Engrg. 164 (1–2) (1998) 121–139.
[21] R. Tezaur, A. Macedo, C. Farhat, R. Djellouli, Three-dimensional finite element calculations in acoustic scattering using arbitrarily shaped convex artificial boundaries, Internat. J. Numer. Methods Engrg. 53 (6) (2002) 1461–1476.
[22] G.A. Kriegsmann, A. Taflove, K.R. Umashankar, A new formulation of electromagnetic wave scattering using an on-surface radiation boundary condition approach, IEEE Trans. Antennas Propagation 35 (2) (1987) 153–161.
[23] X. Antoine, Fast approximate computation of a time-harmonic scattered field using the on-surface radiation condition method, IMA J. Appl. Math. 66 (1) (2001) 83–110.
[24] M. Teymur, Assessment of the surface radiation condition by reference to acoustic scattering by a hard sphere, IMA J. Appl. Math. 48 (3) (1992) 217–241.
[25] M. Teymur, A comparative investigation of the surface radiation condition in electromagnetics, Wave Motion 16 (1) (1992) 1–21.
[26] E. Turkel, C. Farhat, U. Hetmaniuk, Improved accuracy for the Helmholtz equation in unbounded domains, Internat. J. Numer. Methods Engrg., submitted for publication.
[27] M.J. Grote, J.B. Keller, On nonreflecting boundary conditions, J. Comput. Phys. 122 (2) (1995) 231–243.
[28] D. Colton, R. Kress, Inverse Acoustic and Electromagnetic Scattering Theory, second ed., Springer, Berlin, 1998.
[29] P.D. Lax, R.S. Phillips, Scattering Theory, second ed., Academic Press, Boston, MA, 1989.
[30] J. Sanchez-Hubert, E. Sánchez-Palencia, Vibration and Coupling of Continuous Systems, Springer, Berlin, 1989.
[31] I. Stakgold, Boundary Value Problems of Mathematical Physics, vol. II, Macmillan, New York, 1968.
[32] C.H. Wilcox, Scattering Theory for the d'Alembert Equation in Exterior Domains, Springer, Berlin, 1975.
[33] L.F. Kallivokas, J. Bielak, R.C. MacCamy, A simple impedance-infinite element for the finite element solution of the three-dimensional wave equation in unbounded domains, Comput. Methods Appl. Mech. Engrg. 147 (3–4) (1997) 235–262.
[34] O.M. Ramahi, Stability of absorbing boundary conditions, IEEE Trans. Antennas Propagation 47 (4) (1999) 593–599.
[35] C.K.W. Tam, J.C. Webb, Radiation boundary condition and anisotropy correction for finite difference solutions of the Helmholtz equation, J. Comput. Phys. 113 (1) (1994) 122–133.
[36] I. Harari, T.J.R. Hughes, Analysis of continuous formulations underlying the computation of time-harmonic acoustics in exterior domains, Comput. Methods Appl. Mech. Engrg. 97 (1) (1992) 103–124.
[37] M. Abramowitz, I.A. Stegun (Eds.), Handbook of Mathematical Functions with Formulas, Graphs, and Mathematical Tables, Appl. Math. Ser., vol. 55, US Department of Commerce, National Bureau of Standards, Washington, DC, 1972.
[38] L.L. Thompson, P.M. Pinsky, A space-time finite element method for the exterior structural acoustics problem: Time-dependent radiation boundary conditions in two space dimensions, Internat. J. Numer. Methods Engrg. 39 (10) (1996) 1635–1657.
[39] M. Teymur, A note on higher-order surface radiation conditions, IMA J. Appl. Math. 57 (2) (1996) 137–163.
[40] T.L. Geers, Doubly asymptotic approximations for transient motions of submerged structures, J. Acoust. Soc. Amer. 64 (5) (1978) 1500–1508.
[41] R.J. Astley, Infinite elements for wave problems: A review of current formulations and an assessment of accuracy, Internat. J. Numer. Methods Engrg. 49 (7) (2000) 951–976.
[42] R.J. Astley, J.A. Hamilton, Numerical studies of conjugated infinite elements for acoustical radiation, J. Comput. Acoust. 8 (1) (2000) 1–24.
[43] J.L. Cipolla, Axisymmetric modal impedance properties of some infinite element formulatons, Boll. Geofis. Teor. Appl. 40 (1) (1999) 90–91, Supplement.

[44] T.L. Geers, B.J. Toothaker, Third-order doubly asymptotic approximations for computational acoustics, J. Comput. Acoust. 8 (1) (2000) 101–120.
[45] R. Courant, D. Hilbert, Methods of Mathematical Physics, vol. I, Interscience, New York, 1953.
[46] E.W. Weisstein, CRC Concise Encyclopedia of Mathematics, CRC Press, Boca Raton, FL, 1999.